This is a repository copy of *Secondary shock delay measurements from explosive trials*.

White Rose Research Online URL for this paper:
http://eprints.whiterose.ac.uk/105006/

Version: Accepted Version

Proceedings Paper:
Rigby, S.E. and Gitterman, Y. (2016) Secondary shock delay measurements from explosive trials. In: Proceedings of the 24th Military Aspects of Blast and Shock. 24th Military Aspects of Blast and Shock, 19-23 Sep 2016, Halifax, Nova Scotia, Canada. MABS .

SECONDARY SHOCK DELAY MEASUREMENTS FROM EXPLOSIVE TRIALS

S. E. Rigby[1], Y. Gitterman[2]

[1]*Department of Civil & Structural Engineering, University of Sheffield, Mappin Street, Sheffield, S1 3JD, UK;*
[2]*Seismology Division, Geophysical Institute of Israel, POB 182, 71100 Lod, Israel*

ABSTRACT

Following detonation of an explosive material, a series of rarefaction expansion waves collapse inwards from the interface between the explosive and the surrounding air. These rarefaction waves coalesce at the centre of the explosive and reflect as a shock wave. Whilst these successive shocks are small in magnitude compared to the primary shock and are often ignored, the inward reflected shock immediately following the primary shock wave, typically referred to as the 'secondary shock', is a noticeable feature on blast pressure histories and usually arrives after the beginning of the negative phase.

This paper presents results from medium and large scale surface blast tests where accurate measurements of secondary shock delay (time after arrival of the primary shock) are obtained for various explosives at various scaled distances. A method is presented for adjusting the secondary shock delay time by the product of the velocity of detonation divided by the cube-root of the packing density of the explosive. The relationship between this new secondary shock delay parameter and scaled distance is then found to be consistent for all explosives considered. This gives a new empirical method for estimating the yield of an explosive, or determining the velocity of detonation, based only on measurements of the secondary shock delay.

INTRODUCTION

Upon detonation of an explosive material, a high pressure wave, supported by the exothermic detonation of the explosive material, travels through the explosive at a characteristic detonation velocity, V_{od}. Once this wave reaches the edge of the explosive, the reacting high explosive products begin to expand, rapidly accelerating the air to around 10–11 orders of magnitude greater than gravitational acceleration [1]. This causes a primary shock wave to form, which propagates away from the point of detonation. The subsequent expansion of the detonation products results in rarefaction of the interior and the formation of a backwards-moving shock wave that converges on the point of detonation and reflects. This outward-travelling shock wave propagates into the surrounding air following the primary shock and is known as the 'secondary shock'. As this secondary shock reaches the interface between the reaction gasses and the air, a subsequent rarefaction wave is propagated back through the explosive, setting up a tertiary shock. This process is repeated until the energy in the detonation product gas cloud has dissipated [2].

Whilst the tertiary and subsequent shocks are of little importance and are often difficult to measure experimentally, the secondary shock is a common feature in experimental measures of

blast pressure-time histories, typically arriving after the beginning of the negative phase. Despite its clear existence, the secondary shock is often overlooked and there are few studies dedicated to analysis of the secondary shock and its effect. There are a small number of studies reported in the literature where the secondary shock has been accurately measured from experimental trials [3–7]. These will be discussed in more detail in the following section. There are even fewer studies where the secondary shock has been studied analytically. In his seminal work on numerical solutions of spherical blast waves, Brode [2] calculated secondary shock propagation up to distances of several thousand charge radii from the detonation point. Friedman [8] developed equations describing the formation and propagation of the primary and secondary shock, but the analyses were not run past the secondary shock returning to the charge centre.

Recently, Gitterman [3] compiled secondary shock parameters for a number of explosives over a large range of scaled distances, where the scaled distance is given by the distance from the explosive centre to the gauge divided by the cube-root of the charge mass, $Z=R/W^{1/3}$, as is common. The new secondary shock delay parameter δt_{ss} (the time between the main and secondary shocks) was established and analyzed, and a clear correlation was found between the equally scaled - delay ($\delta t_{ss}/W^{1/3}$) and distance. The results indicated that the formation time (i.e. the delay) of the secondary shock is strongly dependent on explosive type, yet reasonably consistent for any given explosive. This paper extends the previous study by including results from smaller scale testing and performing associated numerical analyses to assess the ability of commercial finite element software to predict the secondary shock. The expanded dataset is further analyzed and a new secondary shock parameter is introduced.

EXPERIMENTAL RECORDINGS OF SECONDARY SHOCK DELAY

The following experiments were compiled by Gitterman [3]:

- Two large-scale – 10,240 and 102,080 kg – hemispherical ANFO explosions and one 81,664 kg IMI charge (high explosives provided by Israel Military Industries Ltd., consisting of a mixture of different recuperated high explosives: TNT and gunpowder as major agents, and smaller amounts of Composition B and RDX), conducted by the Geophysical Institute of Israel at the Sayarim Military Range (SMR) in the Negev desert [3]. Secondary shock features were observed from pressure gauges located close to the charge (less than 600 m), as well as from seismic and acoustic sensors deployed up to 20,000 m from the charge centre, giving a range of scaled distances between 2.23–926.46 m/kg$^{1/3}$. A new parameter was introduced, termed the secondary shock delay, δt_{ss}, given as the time between arrival of the primary and secondary shock fronts (see Figure 1).

- Detonation of two 20 ton and one 100 ton (18,200 and 91,100 kg) hemispherical ANFO charges, conducted at Defence Research Establishment Suffield in 1969 and reported by Sadwin and Swisdak Jr. [4]. Incident blast pressure histories were recorded, and scaled distance dependent relations for the arrival time and peak pressure of the secondary shock, among others, were presented. Measurements were taken between 67.4–749.8 m from the centre of the explosive, corresponding to scaled distances of 2.62–16.66 m/kg$^{1/3}$.

- Distant Image and Minor Uncle high explosive tests at White Sands Missile Range in 1991 and 1993 respectively, reported by Reinke et al [5]. These tests consisted of very large (2,210,000 and 2,472,000 kg) hemispherical ANFO charges. Pressure was recorded between 1,500–50,000 m from the charge centre, giving scaled distances of 11.5–383.9 m/kg$^{1/3}$.

- 830 kg cast TNT charges and a 360 kg Composition B charge [9], with pressures recorded between 7–19 m from the charge centre, conducted at SMR in 2008. A small number of secondary shock delays were recorded at scaled distances between 0.74–2.02 m/kg$^{1/3}$.
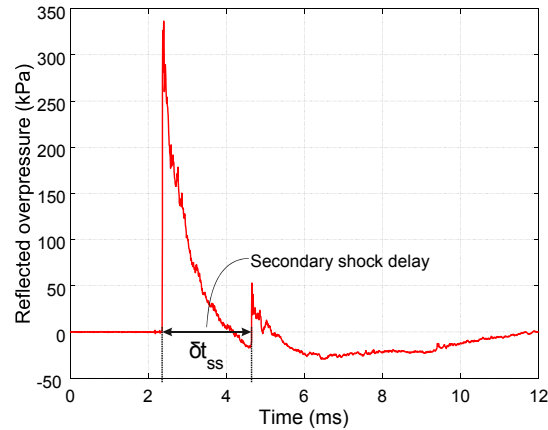
Figure 1: Example reflected blast pressure history showing clear secondary shock features. Secondary shock delay, δt_{ss}, labelled

In addition to these data points, a number of additional smaller-scale experiments are considered for this paper:

- A total of 27 experiments conducted at the University of Sheffield Blast & Impact Laboratory in Buxton, Derbyshire, UK, since 2011 [10–12]. Press-moulded hemispherical charges of PE4 (British equivalent of C4) were detonated on small, sacrificial steel anvils which sat on a flat, rigid, reinforced concrete ground slab. Reflected pressure was recorded at the base of an effectively semi-infinite bunker wall using miniature high pressure Kulite pressure transducers. Pressure was measured between 2–10 m from charges ranging between 0.18–0.35 kg, giving scaled distances between 3.17–15.87 m/kg$^{1/3}$. The example shown in Figure 1 comes from one of these tests.

- Six experiments with the same set up as above in work that is yet to be published on determining far-field TNT equivalence of PETN [13]. Pressure was recorded 2–6 m from 0.25 kg hemispherical charges, giving a range of scaled distances between 3.17–9.52 m/kg$^{1/3}$.

The experiments described above are summarised in Table 1. The packing density, ρ, and detonation velocity, V_{od}, are also given as informed by the suppliers. Explosive properties from Dobratz & Crawford [14] are given where supplier information was not available.

Table 1: Summary of experiments compiled in this article

Explosive	Packing density, ρ (kg/m^3)	Detonation velocity, V_{od} (m/s)	Charge mass (kg)	Number of data points	Sources
ANFO	810–840	4,250–4,400	10,240–2,472,000	107	[3–5]
CompB	1,717	7,980	360	1	[9]
IMI	1,600	7,500	81,664	8	[3]
PE4	1,601	8,193	0.18–0.35	27	[10–12]
PETN	1,770	8,300	0.25	6	[13]
TNT	1,630	6,930	830	5	[9]

Figure 2 shows the compiled scaled secondary shock delays, δt_{ss}, from the experiments described above, plotted against scaled distance. Here, the charge mass for both scaled delay time and scaled distance is divided by the cube-root of the nominal mass of the explosive itself, rather than an equivalent mass of TNT. As previously noted by Gitterman [3] and seen clearly in Figure 2, the data separates into a number distinct groups based on the explosive type, with the grouping for ANFO clear in the main figure and the IMI, PE4, and PETN groupings shown in the sub-figure. It can be seen that the secondary shock delay increases with scaled distance as a result of the higher pressure primary shock propagating faster than the trailing lower pressure secondary shock.

Whilst the values of secondary shock delay for ANFO appear to show a larger spread, particularly at larger scaled distances, it is worth noting that the explosive composition differs significantly between the different tests compiled here (Table 1) and hence the parameters such as density and detonation velocity occupy a broader range. At this stage, it is also worth noting that each point for the PE4 and PETN data sets corresponds to a separate experiment. These data sets, therefore, exhibit test-to-test variations of the experiment itself, whereas the larger scale tests will capture localised variations of the blast wave more so than any test-to-test variance.
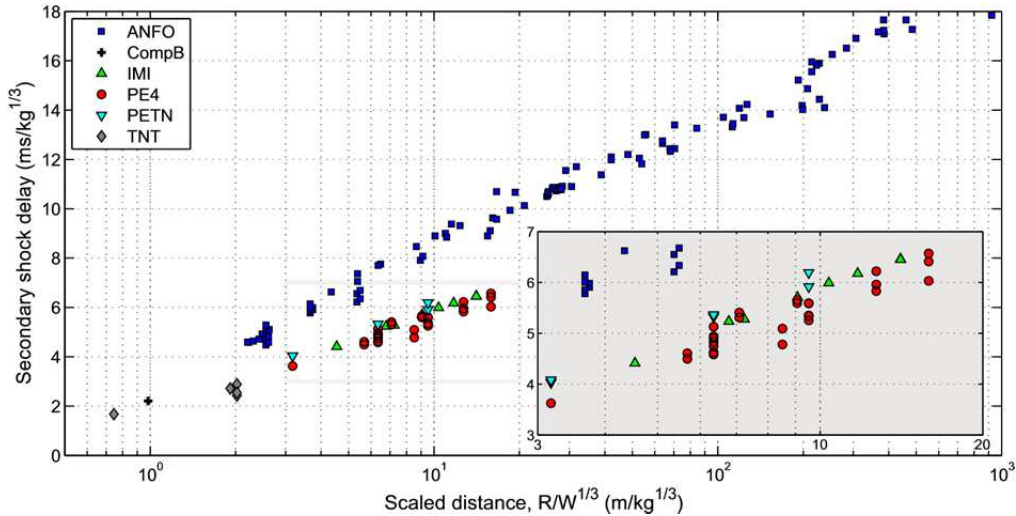
Figure 2: Scaled secondary shock delay versus scaled distance

NUMERICAL ANALYSES

Supporting numerical analyses were conducted using the Multi-Material Eulerian/Arbitrary Lagrangian-Eulerian (MM-ALE) solver in LS-DYNA [15]. Specifically, numerical analyses were performed to evaluate the normally reflected pressure acting at 4, 6, 8, and 10 m from the centre of 250 g hemispherical PE4 explosives. Two models were run for each of the four stand-offs: one with the explosive modelled as PE4 with the same mass as those in the experiments, and one with the explosive modelled as 300 g TNT (representing a TNT equivalence of 1.2). Whilst a TNT equivalence of 1.2 has previously been shown to offer an accurate means for equating a mass of PE4 as a TNT equivalent in terms of positive phase pressure and impulse [10], the effect on the secondary shock when modelling an explosive using a TNT equivalence had not yet been reported.

The explosives were modelled using the Jones-Wilkins-Lee equation of state with parameters given by Dobratz & Crawford [14], and the surrounding air was modelled as an ideal gas. The PE4 was assumed to be identical to C4. The analyses were initialised in 2D axi-symmetry with a radially symmetric mesh whilst the blast wave was propagating through free air. This information was then mapped onto a domain of rectangular 2D axi-symmetric elements immediately prior to impingement onto the rigid target. This was done to minimise advection errors associated with mass transport across element diagonals [16]. The target was modelled using nodal point constraints.

Figure 3 shows the reflected overpressure and reflected specific impulse histories for the 4 m stand-off case. Both models appear to be very accurate for the positive phase of the blast, with the numerical waveforms tracking the experimental waveform almost perfectly up until the beginning of the negative phase. Whilst the peak pressure in the models is under-predicted due to numerical dispersion, as should be expected, the peak impulses of 65.8 and 66.4 kPa.ms for the

PE4 and TNT compare well to the experimentally measured value of 68.8 kPa.ms – differences of 4% and 3% respectively.
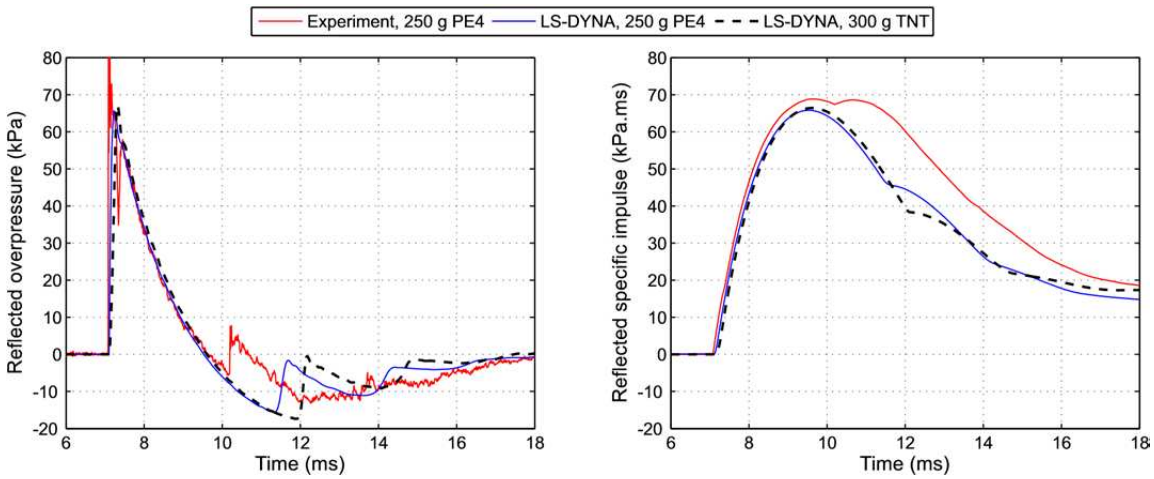
Figure 3: Experimental and numerical reflected overpressure and reflected specific impulse at 4 m stand-off

The negative phase behaviour is less well predicted by the models. In particular, the numerical secondary shock arrives a lot later than the experimental secondary shock and is markedly different depending on explosive type, despite the primary shocks being almost identical. Figure 4 shows compiled experimental and numerical secondary shock delay times. The secondary shock is strongly dependent on the state of the detonation cloud immediately post-detonation; therefore the fact that this behaviour is not captured correctly in the numerical model suggests that the properties of the detonation cloud are not correct. This is at odds with the previous observation of highly accurate positive phase predictions which suggest the explosive parameters are indeed modelled correctly. The cause of this behaviour is unknown and the subject should be studied further.

Whilst the numerical results are not satisfactory in terms of the secondary shock, they do suggest that the secondary shock could be used as an indicator of the state of the detonation products post-detonation. This is explored further in the following section.
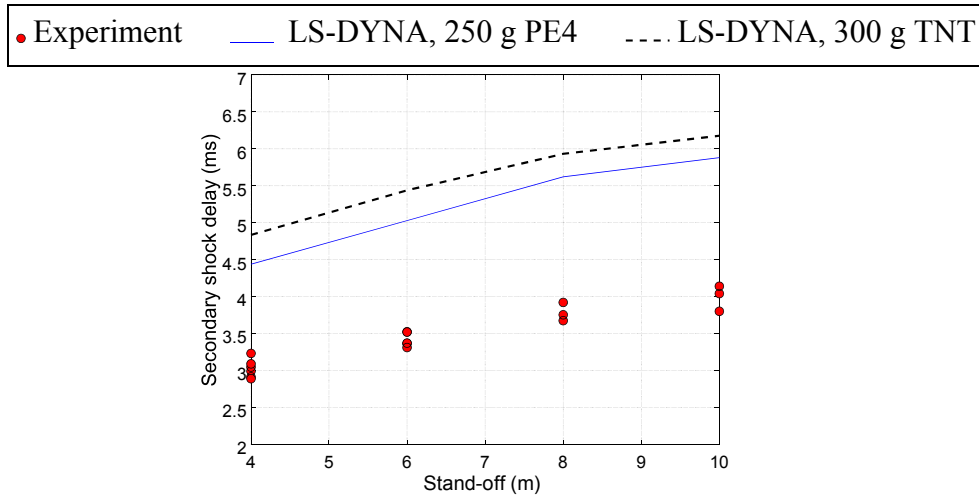
Figure 4: Compiled numerical and experimental secondary shock delays

NEW SECONDARY SHOCK DELAY PARAMETER

Here a new secondary shock parameter, τ_{ss} is introduced, which is given by multiplying the scaled secondary shock delay, $\delta t_{ss}/W^{1/3}$, by the detonation velocity divided by the cube-root of the packing density, $V_{od}/\rho^{1/3}$, i.e.

$$\tau ss = \delta tss Vod/(\rho W)^{1/3} \tag{1}$$

This definition is close to an idea presented in Gitterman [3] that the secondary shock delay correlates with the characteristic time of complete detonation of a finite hemispherical charge. Figure 5(a) shows the compiled new secondary shock delay parameters plotted against scaled distance for the entire experimental dataset discussed previously in this article. It appears as though there is a consistent relationship between Z and τ_{ss} which is independent of explosive type. As such, a least-squares fit was utilised to develop an equation representing this relationship in the form

$$\tau_{ss} = A\log_{10}(Z) + B \tag{2}$$

where A and B are coefficients to be determined from the least squares analysis. It was found that coefficients of 2.45 and 1.36 for A and B offered the best fit, giving an R-squared value of 0.9820. This fit is shown in Figure 5(b).

DISCUSSION

The relationship between Z and τ_{ss} presented in this paper has the following applications: firstly, if an explosion occurs (whether accidental or malicious), and the secondary shock delay is

recorded at some distance from the explosive, the mass of explosive can be determined provided the explosive type is known. If the explosive type is not known, then a number of different possible yields can be easily determined for several common explosives, for example the ones studied in this paper. This could potentially be a valuable diagnostic tool when surveying building damage caused by terror attacks..

Secondly, the relationship outlined above allows experimentalists to determine the velocity of detonation of an explosive material without the requirement for sensitive or specialist equipment to be located close to the explosive charge. Given the density and mass of an explosive, which will be known prior to testing, the detonation velocity can easily be read from Figure 5(b). That the secondary shock delays at scaled distances in excess of 400 $m/kg^{1/3}$ in this article follow the same trends as those of a much nearer-field event extends the remit of this method. Furthermore, as evidenced by the different measurement techniques described by Gitterman [3], the secondary shock delay does not need to be recorded by traditional pressure gauges as it can be determined from seismic and acoustic sensors, as well as the potential for use of optical techniques such as image tracking using high speed video cameras. Finally, the generalised relationship presented in this paper could be used to develop secondary shock predictions for different explosives for use with the existing semi-empirical positive and negative phase predictions found in literature such as UFC-3-340-02 [17].

The main advantage of using secondary shock delay as a metric is that, unlike parameters such as peak pressure or peak impulse, the value of secondary shock delay is typically very well defined and easy to determine. There is less room for interpretation of a secondary shock delay time than there is a backward-fit peak pressure value or an impulse integrated from noisy data. The delay time measurement will not be affected by sensor noise, ringing, or voltage drift; all of which have the potential to render pressure readings unusable. As an example, Figure 6(a) shows the same test as Figure 1 (250 g PE4 at 2 m), but with a fictitious random noise ranging between ±25 kPa added. Shown below this in Figure 6(b) is the temporal gradient of the pressure signal. The arrival times of the primary and secondary shocks are clearly seen as peaks in the data. This gives an irrefutable measure of secondary shock delay; these maxima can be automatically evaluated using programming software such as MatLab, eliminating a potential source of human error.
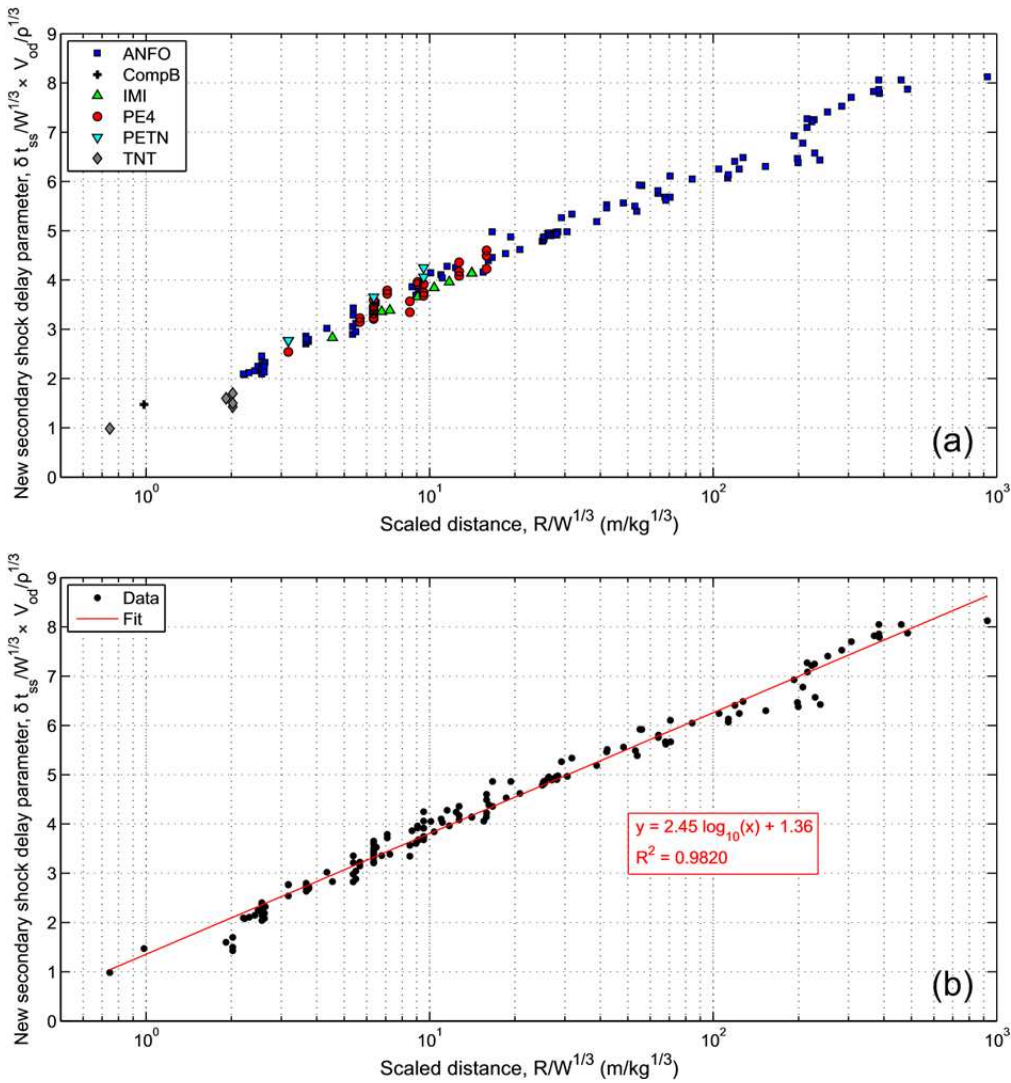
Figure 5: New secondary shock delay parameter, τ_{ss}, for all explosives studied and least-squares fit to data

WORKED EXAMPLES

This section includes several worked examples demonstrating how the applications outlined above would work in practice. Note: secondary shock delay is expressed in seconds.

Example 1: A secondary shock delay of 2.299 milliseconds was recorded 2 m from a hemispherical 250 g PE4 explosion. Estimate the detonation velocity of PE4, given a packing density of 1,601 kg/m^3.

- Scaled distance, $Z = R/W^{1/3} = 2/0.25^{1/3} = 3.175$ m/kg$^{1/3}$

- New secondary shock delay parameter, $\tau_{ss} = 2.45\log_{10}(Z) + 1.36 = 2.589$
- $\tau_{ss} = \delta t_{ss} V_{od}/(\rho W)^{1/3}$, rearranging gives:
- $V_{od} = \tau_{ss} \times (\rho W)^{1/3}/\delta t_{ss}$, therefore
- $V_{od} = 2.589 \times (1601 \times 0.25)^{1/3}/2.299 \times 10^{-3} = 8,299$ m/s
- This is within 2% of the value of 8,190 given in [14].
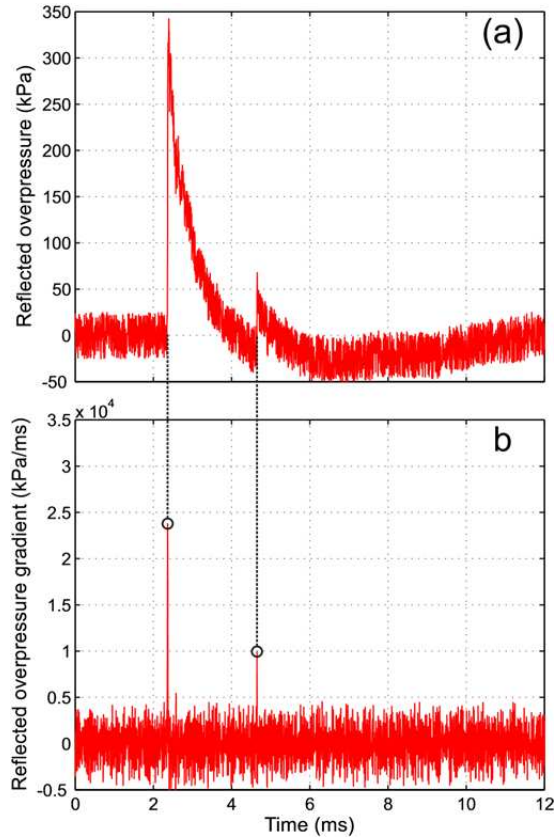
Figure 6: Calculating secondary shock delay from noisy signals

Example 2: A secondary shock delay of 0.235 seconds was recorded 570 m from a hemispherical ANFO explosion. Estimate the yield of the explosive, given a detonation velocity of 4,200 m/s and a packing density of 840 kg/m^3.

- $\tau_{ss} = 2.45\log_{10}(Z) + 1.36 = 2.589$, and
- $\tau_{ss} = \delta t_{ss} V_{od}/(\rho W)^{1/3}$, therefore
- $\delta t_{ss} V_{od}/(\rho W)^{1/3} = 2.45\log_{10}(R/W^{1/3}) + 1.36$.

Rearranging the above in terms of W, gives:

- $W = (\delta t_{ss} V_{od} / (\rho^{1/3} \times (2.45 \log_{10}(R/W^{1/3}) + 1.36)))^3$
- $W = (0.235 \times 4{,}200 / (840^{1/3} \times (2.45 \log_{10}(570/W^{1/3}) + 1.36)))^3$
- Solving iteratively gives $W = 10{,}081$ kg. The actual charge mass used in this test was 10,240 kg. Again, the prediction is within 2% of the experimental value.

Example 3: Calculate the yield from the above example if the explosive was TNT with a detonation velocity of 6,930 m/s and a packing density of 1,630 kg/m^3.

- $W = (\delta t_{ss} V_{od} / (\rho^{1/3} \times (2.45 \log_{10}(R/W^{1/3}) + 1.36)))^3$
- $W = (0.235 \times 6{,}930 / (1{,}630^{1/3} \times (2.45 \log_{10}(570/W^{1/3}) + 1.36)))^3$
- A 29,944 kg TNT explosion would give a secondary shock delay of 0.235 seconds at 570 m stand-off.

CONCLUSIONS

A large number of secondary shock delay times have been compiled for six different explosive types across a wide range of scales and scaled distances. The secondary shock delay exhibits a strong dependence on the explosive chemistry, and the results were seen to lie in distinct bands based on the explosive type used in the testing.

Numerical analyses have shown that, whilst the positive phase of the blast may be well represented by standard modelling techniques, the secondary shock is not well predicted. This suggests that the explosive event delivers the correct energy to the surrounding air, yet the post-detonation behaviour is not captured correctly.

A new secondary shock delay parameter is presented, and a strong correlation is found with scaled distance which is independent of explosive type. This is a potentially very profound finding as it allows us to determine the state of the explosive immediately after detonation whilst still using standard experimental techniques which can be located far from the explosive centre. A number of worked examples are provided to show how the results in this paper can be used to estimate explosive properties based on easily measured experimental data.

REFERENCES

[1]   C. E. Needham. *Blast Waves*. Springer, Berlin, Germany, 2010.

[2]   H. L. Brode. Numerical solutions of spherical blast waves. *Journal of Applied physics*, 26(6):766–775, 1955.

[3]   Y. Gitterman. Secondary shock features for large surface explosions: results from the Sayarim military range, Israel and other experiments. *Shock Waves*, 24(3):267–282, 2014.

[4]   L. D. Sadwin and M. M. Swisdak Jr. Blast characteristics of 20 and 100 ton hemispherical AN/FO charges. Technical Report NOL TR 70–32, United States Naval Ordnance Laboratory, White Oak, MD, USA, 1970.

[5] R. E. Reinke J. A. Leverette, R. A. McCrory. *Chapter 4: Far-field ground motion and airblast measurements*. Report of Experimental Shock Physics Office, Field Command Defense Nuclear Agency, 1993.

[6] Y. Gitterman. Sayarim Infrasound Calibration Explosion: near-source and local observations and yield estimation. In The 2010 Monitoring Research Review: Ground-Based Nuclear Explosion Monitoring Technologies, pages 708-719, Orlando, FL, USA, 2010.

[7] E. M. Fisher and J. F. Pittman. Air blast resulting from the detonation of small TNT charges. Technical Report 2890, United States Naval Ordnance Laboratory, White Oak, MD, USA, 1953.

[8] M. P. Friedman. A simplified analysis of spherical and cylindrical blast waves. *Journal of Fluid Mechanics*, 11:1–15, 1961.

[9] Y. Gitterman and R. Hofstetter. Infrasound calibration experiment in Israel: preparation and test shots. In The 30th Monitoring Research Review on Ground-Based Nuclear Explosion Monitoring Technologies, pages 882–893, Portsmouth, VA, USA, 2008.

[10] A. Tyas, J. Warren, T. Bennett, and S. Fay. Prediction of clearing effects in far-field blast loading of finite targets. Shock Waves, 21(2):111–119, 2011.

[11] S. E. Rigby, A. Tyas, and T. Bennett. Single-degree-of-freedom response of finite targets subjected to blast loading – the influence of clearing. *Engineering Structures*, 45:396–404, 2012.

[12] S. E. Rigby, Fay S.D., Tyas A, Warren J.A., and Clarke S.D. Angle of incidence effects on far-field positive and negative phase blast parameters. *International Journal of Protective Structures*, 6(1):23–42, 2015.

[13] A. Tyas. Unpublished experimental work on TNT equivalence of PETN hemispheres. University of Sheffield.

[14] B. M. Dobratz and P. C. Crawford. LLNL explosives handbook - properties of chemical explosives and explosive simulants. Technical Report UCRL 52997, Lawrence Livermore National Laboratory, University of California, CA, USA, 1985.

[15] J. O. Hallquist. *LS-DYNA Theory Manual*. Livermore Software Technology Corporation, CA, USA, 2006.

[16] S. E. Rigby, A. Tyas, T. Bennett, S. D. Fay, S. D. Clarke, and J. A. Warren. A numerical investigation of blast loading and clearing on small targets. *International Journal of Protective Structures*, 5(3):523–574, 2014.

[17] US Department of Defence. *Structures to resist the effects of accidental explosions*. US DoD, Washington DC, USA, UFC-3-340-02, 2008.